View Online

Ab initio simulation of UV/vis absorption spectra for atmospheric modeling: method design for medium-sized molecules

Anna Melnichuk,* Ajith Perera and Rodney J. Bartlett

Received 28th January 2010, Accepted 16th April 2010
DOI: 10.1039/c001906b

A procedure is presented to obtain accurate absorption cross-sections for dissociative excited states. The focus is the ability to approximate many vibrational degrees of freedom while maintaining a minimal computational time. The vibrational Hamiltonian for bound and unbound surfaces is solved within a discrete variable representation (DVR) framework. Properties and energies of excited states are computed using electron correlated singles and doubles equation-of-motion (EOM-CCSD) and similarity transformed equation-of-motion (STEOM-CCSD) methods as implemented in ACESII. The novelty of this procedure is that it is designed to work for medium-sized molecules (size limited by the choice of electronic structure method, not vibrational degrees of freedom) with one or more photodissociation pathways. The theoretical absorption cross-section of NaOH is presented as a small-scale example.

Published on 15 June 2010 on http://pubs.rsc.org | doi:10.1039/C001906B
Downloaded on 17 August 2010

1 Introduction

The photodissociation rates of volatile organic and inorganic compounds are critically important in modeling the composition of the atmosphere, in addressing global warming, ozone depletion, and other phenomena. The absorption cross section in the spectral range of solar flux is needed to calculate the photodissociation rate constant

$$J = \int_\lambda \phi_\lambda \sigma_\lambda F_\lambda \, d\lambda \quad (1)$$

where λ is the incident wavelength, σ is the absorption cross section, ϕ is the quantum yield of photodissociation and F is the solar actinic flux.

The photodissociation rate constant and its dependence on temperature can be measured provided a pure sample is obtained and the absorption cross section at various temperatures is known.[1,2] The pure sample condition becomes increasingly difficult to satisfy as the size, complexity and stability of the compound in question impede attempts to synthesize it. Currently, the absorption cross sections that are used to determine the photodissociation rates of complex or unstable molecules are unknown and are crudely estimated. For example, the photodissociation rate values for organic peroxides are taken from the absorption cross sections of hydrogen peroxide and methyl peroxide simply due to their experimental availability, bypassing the difficulties in obtaining the experimental cross sections of the actual molecules.[3] Using estimated values as opposed to the true values can lead to serious inaccuracies in the steady state models of the atmosphere.

Normally, when an absorption cross section is calculated with *ab inito* methods a vibronic model can be used to include some molecular motion. In order to compute a photodissociation absorption cross section for relatively large species several complications of the vibronic model need be resolved. None of the currently available software can properly handle the dissociative excited state surface, and few can correctly handle a torsional potential since it does not naturally lend itself to a quadratic or quartic expansion but rather should be expanded with a set of trig functions.[4,5] Even if this model is made to work with the types of PESs involved in photodissociation, there is still the aspect of finding the roots of a very large matrix which may not be sparse when there are many strong vibronic couplings present.

The most widely used programs that have the capability to simulate an absorption spectrum are VIBRON[6] and HOTFCHT.[7] All of these programs require a calculation of the harmonic normal modes of the absorbing state which works well enough for excited state potential energy surfaces which have a stationary point, but do not perform well for dissociative potential energy surfaces. The LEVEL[8] program works for bound and quasi-bound potentials and has been successfully applied to a variety of diatomic molecules.

We propose a method for computing absorption cross sections for dissociative surfaces which are geared toward describing a larger molecule with more than 10 vibrational degrees of freedom. As an illustration of the methodology we chose a small molecule, sodium hydroxide. Photodissociation of gaseous NaOH as well as other sodium oxide compounds is an important atmospheric process in the mesosphere,[9] and the absorption cross sections leading to photodissociation have been obtained experimentally using flame absorption[10] and laser spectroscopy.[11] The pertinent experimental results are from the laser spectroscopy study of Self and Plane 2002. No high level *ab inito* study of the absorption cross section of NaOH has been done previously.

In this study we use electron-correlated size extensive coupled cluster methods[12–21] for all of the geometry optimizations and excited state calculations. We will be comparing results from the equation-of-motion singles and doubles method, EOM-CCSD,[22] the similarity transformed equation-of-motion method, STEOM[23] and direct energy differences between states of different symmetries, as implemented in ACES II,[24] using a variety of basis sets.

Quantum Theory Project, University of Florida, Gainesville, FL 32601. E-mail: melnichu@qtp.ufl.edu

 This journal is © the Owner Societies 2010

View Online

Published on 15 June 2010 on http://pubs.rsc.org | doi:10.1039/C001906B
Downloaded on 17 August 2010

2 Methods

The discrete variable representation (DVR) method[25] has been used to solve the vibrational Hamiltonian for a variety of small chemical compounds provided a potential energy surface is known with up to N = 16 vibrational degrees of freedom.[26–28] It can be used to find vibrational wavefunctions on a dissociative surface.[29,30] DVR works by a numerical discretization of the kinetic energy operator and the potential into N segments. The detailed derivation of the DVR using the Fourier grid Hamiltonian method can be found elsewhere.[29,31] The discretized form of the kinetic energy operator is shown below where m is the reduced mass and Δx is the size of the grid on which the potentials are placed.

$$T_{ii'} = \frac{\hbar^2}{2m\Delta x^2}(-1)^{(i-i')} \times \begin{cases} \frac{\pi^2}{3} & \text{for } i = i' \\ \frac{2}{(i-i')^2} & \text{for } i \neq i' \end{cases} \quad (2)$$

The Hamiltonian that is diagonalized is shown below where V is the potential function used to fit the *ab intio* data points. The Hamiltonian below is in atomic units.

$$H_{ii'} = T_{ii'} + V_{ii'}\delta_{ii'} = \frac{(-1)^{(i-i')}}{2\mathrm{d}x^2} \times \left\{ \begin{cases} \frac{\pi^2}{3} & \text{for } i = i' \\ \frac{2}{(i-i')^2} & \text{for } i \neq i' \end{cases} \right\} + V_{ii'}\delta_{ii'} \quad (3)$$

The results are sensitive to the resolution of the grid. Since this is a very fast calculation, it is easy to vary the number of grid points until the eigenvalues in the energy range of interest converge. In this work, 501 grid points are enough to reach convergence.

One can rewrite eqn (1) to include the temperature dependence of the photodissociation rate constant:

$$J = \int_\lambda \phi_\lambda \sigma_{\lambda,T} \mathrm{F}_\lambda \mathrm{d}\lambda \quad (4)$$

where the temperature dependence is added *via* the absorption cross section term. The absorption cross section can be written as:

$$\sigma(\lambda, T) = \sum_k^K \{\langle \Psi^k | \mu | \Psi^0 \rangle \sum_{m=0}^M \sum_{n=0}^{N(T)} \langle \Phi_k^m | \Phi_0^n \rangle\} \quad (5)$$

where m is the electronic transition moment obtained from the electronic wavefunctions Ψ, and Φ are the vibrational wavefunctions. The summations are over K-electronic excited states, M-vibrational states on the excited PES and N-vibrational states on the ground PES where $N(T)$ is the maximum occupied vibrational levels at temperature, T. The temperature dependence of the absorption cross section comes from varying the population of the ground state vibrational energy levels. EOM-CCSD is used to compute the electronic transition moment and a locally developed DVR code is used to compute the Franck–Condon integrals. Emphasis is also placed on creating a "black-box" program such that any user familiar with *ab initio* software can obtain a photodissociation cross section for his or her molecule of choice.

An alternative way to find Franck–Condon integrals on a dissociative potential can be accomplished by constructing the ground state wavefunction and propagating it on the dissociative surface.[32] There is not evidence yet to suggest one approach is better than the other, though this alternative will be incorporated as an option for the user.

In order to facilitate comparison between the experimental and the theoretical absorption cross sections it is best to express all intensities as unit-less oscillator strengths as opposed to transition dipole moments. The relationship between the two quantities is:

$$f_{0k} = \left\{\frac{8\pi^2 m_e c g_n}{3he^2}\right\} \omega_{0k} \mu_{0k} \quad (6)$$

ω_{0k} is the excitation energy, μ_{0k} is the dipole strength, c is the speed of light, e is the elementary charge, m_e is the mass of an electron, h is the Planck constant, and g_n is the electronic degeneracy of the excited state.

The experimental data may also be expressed as the oscillator strength[33] provided that the molar extinction coefficient is known.

$$f_{0k} = \left\{\frac{2303 m_e c^2}{\pi N_\mathrm{A} e^2}\right\} F \int_{\omega_1}^{\omega 2} \varepsilon \mathrm{d}\omega \quad (7)$$

Here, N_A is Avogadro's number, F is the correction for the refractive index, which can be set to 1 since this applies to a diffuse gas, and ε is the molar extinction coefficient in the units of L/mol·cm. The quantities obtained from eqn (6) and (7) are the experimental and theoretical vertical excitation intensities which may be compared and the agreement is known to be good based on examples currently found in the literature.[34–36] No comprehensive benchmark studies of calculated oscillator strengths at the coupled-cluster level of theory have been presented but will be forthcoming.

Care must be taken to properly combine the electronic structure results (oscillator strength) with the DVR results (Franck–Condon) such that both are expressed as a function of ω and lie on the same grid. There are several ways to achieve this. One way is described here.

Solving the Hamiltonian as written in eqn (3) will produce the following set of Franck–Condon integrals:

$$FC_{im} = \left\{\sum_j \phi_{mj}\phi_{ji}\right\}^2 \quad (8)$$

where ϕ_{mj} is the eigenvector corresponding to the mth energy level of the ground state potential energy surface and ϕ_{ji} is the eigenvector corresponding to the ith energy level of the excited state potential energy surface. These integrals are normalized such that $\sum_i FC_{im} = 1$. The difference of eigenvalues for the ground and excited state are used to build the ω_i vector: $E_i - E_k = \omega_i$.

The oscillator strengths are calculated as a function of geometry for each electronic transition. However, only the value at the equilibrium geometry corresponds to the experimental value determined using eqn (7), which is an integral of the cross section. What is needed is a way to map the oscillator strength value to the area of the cross section, preferably in *cgs* units. First, rearrange eqn (7) to reflect the *cgs* units:

$$f_{0k} = \left\{\frac{m_e c^2}{\pi e^2}\right\} F \int_{\omega_1}^{\omega 2} \sigma \mathrm{d}\omega \quad (9)$$

View Online

Published on 15 June 2010 on http://pubs.rsc.org | doi:10.1039/C001906B
Downloaded on 17 August 2010

where σ is the absorption cross section in $cm^2/molecule$. Now, rearrange to solve for σ discretely:

$$\tilde{\sigma}_i = \left\{\frac{\pi e^2 g n}{m_e c^2}\right\} \frac{F_i}{\omega_{i+1} - \omega_i} \quad (10)$$

Note that this $\tilde{\sigma}$ is a discrete electronic part of the total σ. The ω in the denominator comes from the eigenvalues of the DVR Hamiltonian. The oscillator strength is also discrete and obtained from *ab initio* calculations which is why g_n appears in this equation. At this point, F_i is the oscillator strength which corresponds to each $m \rightarrow i$ transition and is estimated by a weighted average oscillator strength, $\bar{f}_i$:

$$\bar{f}_i = \frac{\sum_j f_i \times |\phi_{mj}\phi_{ji}|}{\sum_j |\phi_{mj}\phi_{ji}|} \quad (11)$$

Combining eqn (10) and (11) allows the electronic part of σ to be placed on the same grid as the Franck–Condon part of σ such that the largest contribution to F_i arise from the portions of the oscillator strength surface with the greatest Franck–Condon overlap. The total absorption cross section for each electronic transition which can be compared with experiment is then obtained by combining the electronic and vibrational parts:

$$\sigma_{0k} = \sum_i \sigma_i \times \sum_m c_m^T F C_{im} \quad (12)$$

The subscript m will be greater than one when more than one ground state vibrational energy level is populated. The population of the m-states are weighted by a set of temperature-dependent constants c_m, which correspond to the Boltzmann distribution at a given temperature. In the case of $T = 0$ K, m will always be set to 1 corresponding to the first vibrational level.

The final cross sections for each kth excited state are to be convoluted to obtain a theoretical spectrum in the desired spectral range.

In order to calculate the absorption cross section for large molecules several simplifications need to be made. The recurring theme is trying to remove as many non-vital vibrational degrees of freedom as possible. These assumptions are explained below and will be illustrated throughout the NaOH example.

I Consider the dissociative coordinate as the primary coordinate

This is the obvious choice since we are initially interested in those cross sections which lead to dissociation. This method can be extended to use any degree of freedom as the primary coordinate.

II Compute the absorption cross section of the primary mode

This will be the zeroth-order solution. The discrete variable representation method (DVR) is used to compute the Franck–Condon overlap integrals for a dissociative mode.

III Consider only those vibrations which are significantly thermally populated

In practice, this would involve a subset of vibrations of energy equal or lower than the energy of the stretch along which dissociation takes place. By *equal* we mean within some tolerance which is optimal for a given temperature. For example, if one is interested in going to very high temperatures, modes higher in energy than the primary mode should be considered.

IV Determine the impact each secondary mode has on the excitation energies of interest as well as the corresponding dipole transition moments

If the impact is less than some tolerance, remove that normal mode from the subset. This will now define the subset of secondary modes. Any degree of freedom which is not explicitly a part of the secondary modes' subset will be relaxed in all partial geometry optimization calculations so that any small effect of these modes can be reflected in the final answer.

V Add the effects of other degrees of freedom by perturbing the primary mode ground state and excited state potentials

This can be done by extrapolating or fitting the curves used to determine the impacts in step *IV*.

VI Temperature effects can be introduced at this stage

This step involves redistributing energy quanta among the vibrational levels of the primary mode and the various secondary modes.

One consistency check for the procedure outlined above is to use eqn (7) or (9) to find the oscillator strength once the calculated absorption cross section is obtained. If the fits to the PES are adequate and the grid is fine enough, the f_{DVR} should be close to the calculated f for each transition. Furthermore, improving upon fits to the potentials (by using more points or a better analytical fitting function for example) as well as increasing the resolution of the grid should converge the f_{DVR} to the correct value.

3 Results and discussion

3.1 Results I: electronic structure

The starting point for calculating an absorption spectrum is to begin with single point vertical excitation energies. From the energy range of the experimental spectrum in Fig. 1, we see that three low energy excited states are required to create a theoretical spectrum in the near UV spectral range. These states, their symmetry and character are listed in Table 1. The error bars from the experimental data show a great deal of uncertainty in the intensity especially in the peak at 220 nm. In this example the agreement between the calculated and the theoretical oscillator strength is not as good as it has been for other molecules found in the literature[34–36] for transitions to bound excited states. A high resolution absorption cross section of NaOH would be desirable to obtain for comparison. As it presently stands, the calculated oscillator strength is about two times greater than the experimental value.

The geometry is optimized at the CCSD level of theory using the POL basis set.[37] The R_{NaO} = 1.9493 Å and R_{OH} = 0.9589 Å. The best available experimental NaOH geometry[38] is R_{NaO} = 1.9500 Å. This geometry is also in good agreement with the geometries listed in the work of Lee *et al.* who employ a variety of high-end methods and basis sets[39] which suggests that CCSD/POL is adequate to proceed as far as geometry is concerned. Keeping in mind that the method outlined below is geared for larger molecules, the best optimized geometry will often be a DFT geometry done with a modest basis set.

 This journal is © the Owner Societies 2010

View Online

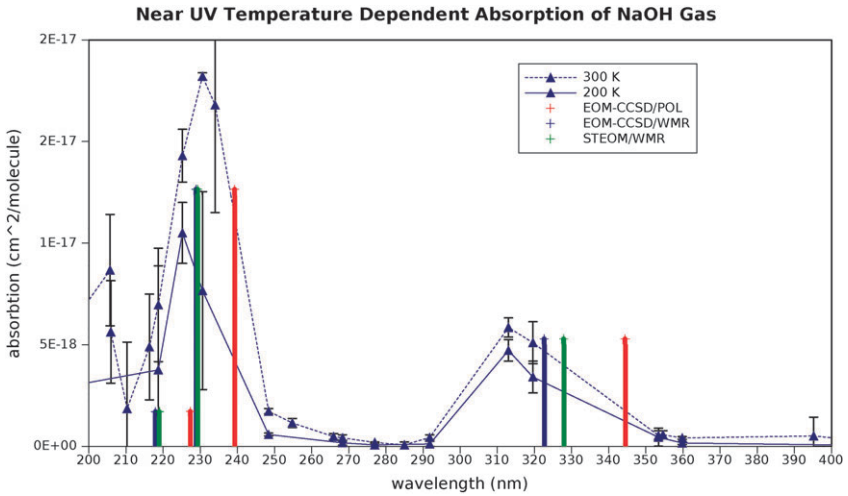

Fig. 1 The POL basis set does a reasonable job of describing the Rydberg excited states in the 220 nm region but it underestimates the energy gap of the valence state. The results from EOM and STEOM calculations with the WMR basis are in good agreement with each other as well as with the experiment. The dipole transition moments remain largely unaffected by the choice of basis set. Vertical excitation intensities are approximate but reflect the theoretical relative intensities.

Table 1 Characteristics of the low energy excited states of NaOH. The calculated values for oscillator strength shown here are multiplied by the applicable electronic degeneracy value. Since the experimental peak from states B and C is unresolved, it needs to be compared to the sum of calculated oscillator strengths for B and C states. The experimental values were obtained from the results reported by Self and Plane

Calculated excited states for NaOH							
State	Symmetry	Character	Type	Electronic degeneracy	EOM-CCSD/ POL (nm)	*f* calc.	*f* exp.
A	$^1\Sigma(0) \rightarrow {}^1\Pi(1)$	Valence	$\pi \rightarrow \sigma^*$	2	344.5	0.054	0.017
B	$^1\Sigma(0) \rightarrow {}^1\Pi(2)$	Rydberg	$\pi \rightarrow \sigma^*$	2	239.2	0.092	0.060
C	$^1\Sigma(0) \rightarrow {}^1\Sigma(1)$	Rydberg	$\pi \rightarrow \pi^*$	1	227.3	0.026	

Excitation energies calculated using the EOM-CCSD method and POL basis set have proven to be a good choice for describing excitation energies and transition dipole moments.[37] Since NaOH is a small molecule, we are also able to calculate the spectrum with the aug-cc-pVXZ (X = D,T)[40,41] basis sets of Dunning and with the WMR[42] basis set of Widmark. This may not be possible to do for the large molecules that are our objective, so we will always present the EOM-CCSD/POL result as an expected electronic structure level of accuracy along with any energy corrections made to it based on the results from a more complete basis set calculation. The best results are shown in Fig. 1 and a comprehensive list of results is summarized in Table 2.

It should be noted that for both EOM and STEOM calculations the mean average deviation is on the order of 0.1 eV. However, the error in the calculated absorption cross section is

Table 2 Detailed excitation energy using the EOM-CCSD and STEOM methods with a variety of basis sets. Mean average deviation (MAD) values and experimental values of Self and Plane are also shown

Near-UV excitation energies for NaOH											
EOM-CCSD											
	POL		aug-cc-pVDZ		aug-cc-pVTZ		WMR		MAD		Exp.
State	eV	nm	eV	nm	eV	nm	eV	nm	eV	nm	nm
A	3.60	344.50	3.65	340.10	3.81	325.70	3.84	322.70	0.10	9.00	313
B	5.18	239.20	5.18	239.30	5.34	232.10	5.42	228.30	0.10	4.50	230
C	5.45	227.30	5.45	227.50	5.61	220.90	5.70	217.90	0.10	4.00	225
STEOM-CCSD											
	POL		aug-cc-pVDZ		aug-cc-pVTZ		WMR		MAD		Exp.
State	eV	nm	eV	nm	eV	nm	eV	nm	eV	nm	nm
A	3.53	351.10	3.58	346.50	3.76	329.40	3.78	327.90	0.11	10.10	313
B	5.15	240.60	5.16	240.20	5.30	233.70	5.41	229.30	0.10	4.40	230
C	5.26	235.60	5.44	227.70	5.59	221.70	5.66	218.90	0.14	5.70	225

Published on 15 June 2010 on http://pubs.rsc.org | doi:10.1039/C001906B
Downloaded on 17 August 2010

View Online

Published on 15 June 2010 on http://pubs.rsc.org | doi:10.1039/C001906B
Downloaded on 17 August 2010

sensitive to the spectral range: the lower energy wavelengths carry a higher error than the higher energy wavelengths as reflected in the MAD values for the energies in nanometer units. Since there are no significant differences between STEOM-CCSD and EOM-CCSD methods for the excited states considered in this work, EOM-CCSD/POL is used in all subsequent calculations with the final energies of the calculated spectrum shifted to the best results from Table 2. The energy adjustments for the absorption peaks are: −21.8 nm for the A state, −9.9 nm for the B state and −9.4 nm for the C state.

There is no reason to suppose that doubly excited states are significant contributors since the average excitation level (AEL)[22] is not greater than 1.07 in any of the EOM-CCSD calculations for the excited states considered.

3.2 Results II: absorption cross section model

This portion of the results section will illustrate the validity of assumptions made in the methodology section using NaOH as an example.

I Consider the dissociative coordinate as the primary coordinate

Fig. 2 shows the behavior of the low energy excited states as a function of distance between the sodium and oxygen atoms. Eleven single point calculations are performed for the distances ranging from 1.7 Å to 5.0 Å. The energy surfaces are computed using CCSD and EOM-CCSD methods with a restricted Hartree–Fock (RHF) reference in the vicinity of the equilibrium geometry and an unrestricted Hartree–Fock (UHF) reference past the Na–O distance of 2.5 Å at which the bond begins to break. Energy data points at 2.5 Å are computed using both RHF and UHF reference functions and an average value was taken to fill in the small discontinuity. The CCSD UHF-RHF energy gap at Na–O distance of 2.5 Å for the ground state PES is 0.23 mH, for the excited state A it is 4.2 mH, and for states B and C it is 7.2 mH.

The valence state is purely dissociative and the Rydberg states are weakly bound. The ground state surface is fit with a Morse potential with the unbound limit set to the sum of the calculated energies of Na and OH radicals (shown as a point at 6.0 Å in Fig. 2). The excited state surfaces are fitted with eqn (13) which allows a good fit for a fully dissociative surface, as well as for a weakly bound surface by setting parameter B to zero.

$$V(x) = A + Bx^{-3} + C\exp(-Dx) \quad (13)$$

The R^2 values of the fits are greater than 0.998 with the worst fit being the Rydberg states due to a small energy gap at the UHF-RHF junction on the energy surfaces. The dipole transition moments are fit using a 6th order polynomial.

II Compute the absorption cross section of the primary mode

At this point, a zeroth-order approximation to the spectrum may be determined. Since the primary mode chosen was a zeroth-order dissociative mode, the theoretical spectrum will have the form of a continuum cross section centered at the vertical excitation of the equilibrium geometry augmented by the dipole transition moment intensity. One can also make a different choice for the primary mode and let it be the bending coordinate, in which case the spectrum will have fine structure of the vibronic progression but lose the broad continuum peak. Since the experiment was not done at a high enough resolution to yield vibronic peaks and we are interested in photodissociation the choice of primary mode remains the Na–OH stretch.

Using the above-mentioned fitting parameters for the energy and dipole strength surfaces the cross section is calculated using a DVR program implemented in FORTRAN specifically for this purpose. The resulting cross section is shown in Fig. 3.

The energy adjustments from POL to the WMR basis set are as follow: A (−21.8 nm), B (−9.9 nm), and C (−9.4 nm). These energies will be used for the rest of the data.

III Consider only those vibrations which are significantly thermally populated

The calculated absorption cross section coming from the primary mode alone is in fairly good agreement with the experimentally obtained cross section. It may be sufficient for this molecule. To further improve the results we need to look at the other vibrational degrees of freedom and what (if any) effect they have on the cross section.

Including the effects of other vibrational modes to the dissociative mode will broaden the energy range of each peak as well as make the intensities more representative of what is experimentally observed. For example, this step would be vital in getting an accurate absorption cross section for an electronically forbidden excited state which is vibronically allowed.

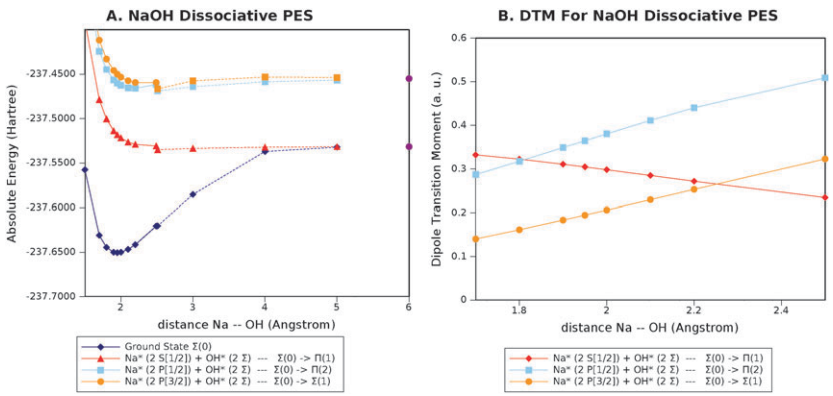

Fig. 2 Energies and dipole transition moments of NaOH along its dissociative coordinate. Solid lines for RHF solutions and dashed lines are UHF solutions. The points at 6.0 Å represent the total energies of the dissociated products. The are no surface crossings observed.

 This journal is © the Owner Societies 2010

View Online

Published on 15 June 2010 on http://pubs.rsc.org | doi:10.1039/C001906B
Downloaded on 17 August 2010

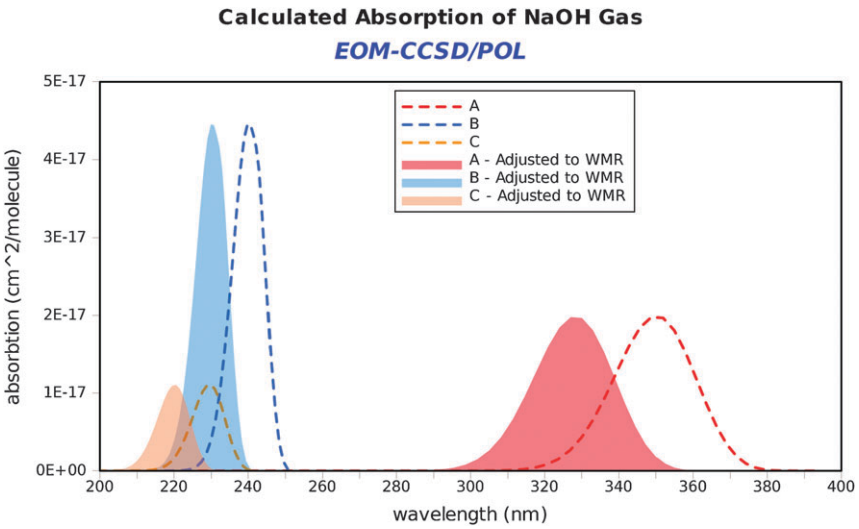

Fig. 3 These cross sections are obtained from the FC overlap between the ZPE vibrational wavefunction of the ground state and the dissociative continuum of the exited states weighed by the dipole transition moment. The surfaces are computed at the EOM-CCSD/POL level of theory and the resulting cross sections are shown as dashed lines. Only the energies are adjusted to the best calculated values from Table 2

Vibrational energies can be found in two ways: 1) harmonic frequencies are calculated using ACES II and 2) anharmonic frequencies are determined from DVR. These values are relatively consistent with each other as well as with experimental data as listed on Table 3. Furthermore, these values are consistent with the results of Lee and Wright who employ a variety of methods and basis sets. The only exception is the experimental bending mode which agrees poorly with calculations in this paper and the values calculated in the paper of Lee and Wright. The experimental frequency should be less than the computed harmonic value and this discrepancy should be reconciled in the future. However, this small difference has no significant effect on the current analysis.

The bending mode is the only low energy mode in this molecule and it will be considered in the next steps. The OH stretching mode is too high in energy to be significantly populated and have an impact on the absorption cross section so it will not be included. The stretching mode has considerable anharmonic character so that the Morse potential fit to the ground state PES provides better agreement with the experimental frequency than with the *ab initio* result.

The bending mode is fit to a quartic potential. The difference in vibrational energy frequencies between the *ab inito* and the DVR values is 35 wavenumbers for the stretching mode which is attributed to anharmonicity of the PES. The bending mode, better described by a harmonic potential, yields a much smaller error between the *ab initio* and the DVR values. Energy errors for vibrational modes on the order of 50 wavenumers introduce less than 0.5 nm error to the absorption cross section in the UV/vis spectral range.

IV Determine the impact each secondary mode has on the excitation energies of interest as well as the corresponding dipole transition moments

In case of NaOH, the bending mode is the only one selected to be in the secondary-mode set. For larger molecules, there will be more low-energy vibrational degrees of freedom to consider so further analysis of normal modes is needed to identify the important degrees of freedom. Inclusion of vibrational modes which strongly couple to the excited state potential energy surfaces is vital for an accurate absorption cross section. Emphasis is placed on the screening being both quick and accurate to minimize the number of *ab initio* calculations that need to be performed. This involves picking each mode in the second set and calculating a few key points along its surface. For each set of points the impact of the molecular geometry deformation along a particular mode on the excitation energy and the dipole transition moment is determined.

The number of actual calculations can be optimally minimized to a few key points on a surface: *cis* and *trans* conformers for dihedral rotation modes, a $\pm$ 30 degree deformation in each direction is appropriate for bending modes and $\pm$ 0.5 Å for stretching modes. Since this approach is still in the testing stage, the above parameters are not to be

Table 3 Characteristics of the vibrational frequencies of NaOH. CCSD/POL frequencies were done at the CCSD/POL optimized geometry. The CCSD/POL potential was used to compute the DVR frequencies

Calculated harmonic and anharmonic vibrational modes for NaOH

Mode	Symmetry	Type	CCSD/POL (cm^{-1})	DVR (cm^{-1})	Exp.(cm^{-1})[a]	Comments
1	Π	Bend	272.31	284.7	337	Include.
2	Σ	Na–O Str.	559.83	526.6	540	Primary mode.
3	Σ	O–H Str.	3969.79	—	3637	Exclude.

[a] Experimental data from Acquista *et al.*[43]

View Online

Published on 15 June 2010 on http://pubs.rsc.org | doi:10.1039/C001906B
Downloaded on 17 August 2010

taken as absolutes but as a staring point. Symmetry and breaking thereof will need some attention paid to it since symmetric modes and asymmetric modes have different behaviors. Furthermore, there are special vibrational modes that need to be taken into consideration like the umbrella mode of ammonia or the ring-breathing mode of benzene.

The first step is to get a list of vibrations which have the most impact and to exclude the ones that have little or no effect. If there is a reason and capability to do more points on the surfaces which matter most, then computer time may be allocated more efficiently to get better surfaces for modes which have a greater impact. Table 4 shows how this procedure works for the bending mode of NaOH.

It is clear from Table 4 that the error in energy of the zeroth-order cross section (Fig. 3) is no grater than 10.8 nm. The lower energy valence excited state is most affected by the bending mode and the errors in the Rydberg states are more tolerable. The dipole transition moment for the A and B states is significantly affected by the bending mode which would have impact on intensities. Fig. 4 shows the energy surfaces and the dipole transition moment surfaces as a function of the bending mode while keeping the R_{NaO} at it equilibrium value and relaxing the R_{OH}.

For a small molecule such as sodium hydroxide it is easy to compute several more points along the bending mode, but this is not necessary to do since we are only interested in the range of the potentials which are close to the equilibrium. If a high temperature spectrum were of interest where a significant fraction of higher vibrational levels are populated, then it would make sense to have more points. The agreement between the DVR vibrational energy for this mode and the *ab initio* frequency suggests that three points provide a good enough fit. A large discrepancy between the energy values would be a signal to do more points for a better potential.

V Add the effects of other degrees of freedom by perturbing the primary mode ground state and excited state potentials

The fitting parameters of the energy surfaces and the dipole transition moments for excited and ground states are used to perturb the zeroth-order dissociative state and recalculate Franck–Condon overlaps. This calculation is done at two points as illustrated in Fig. 5: the original equilibrium

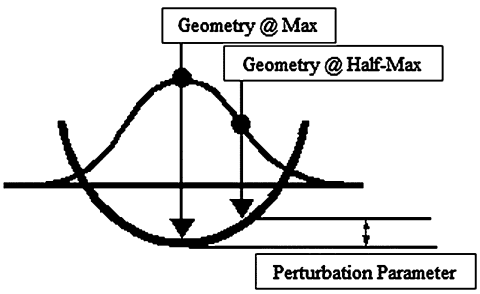

Fig. 5 This is a cartoon of a vibrational wavefunction in a potential (in this case the potential of the bending mode). The change in the surface energy between the equilibrium geometry and the geometry of the half-maximum is what is added onto the zeroth-order dissociative potential for the ground and excited states. The dipole strength potential is multiplied by the fraction of the $DTM_{Half-Max}/DTM_{Max}$.

Table 4 The impact the bending normal mode has on the excited state potential energy surfaces and the dipole transition moments. Impacts for excitation energies are calculated by taking the standard deviation. The dipole transition moment impacts are calculated by taking the ratio of equilibrium value (DTM_{180}) to the other values (DTM_{120} and DTM_{240}) and then taking the standard deviation of the ratios. The equilibrium geometry values are those where the angle is 180 degrees and deviation from equilibrium breaks the electronic degeneracy of the A and B states

Bending mode impact on excitation energy and dipole transition moment						
Excited State	A	B	C	A′	B′	Na–O–H Angle
Excitation	325.8	237.8	232.1	349.7	245.9	120
Energy	344.5	239.3	227.4	344.5	239.3	180
(nm)	325.8	237.8	232.1	349.7	245.9	240
Impact (nm)	**10.80**	**0.86**	**2.71**	**3.00**	**3.81**	
Dipole	0.66	0.03	0.13	0.34	0.02	120
Transition	0.30	0.05	0.19	0.30	0.05	180
Moment (a.u.)	0.66	0.03	0.13	0.34	0.02	240
Impact	**0.69**	**0.23**	**0.18**	**0.08**	**0.35**	

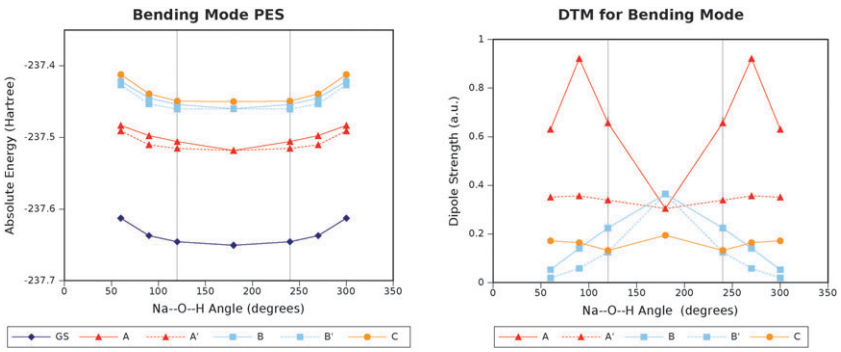

Fig. 4 Energies and dipole transition moments of NaOH along its bending coordinate. The points which are listed in the table are the three points encompassed by the vertical lines. Several more points were done for completeness but were not necessary for accuracy.

 This journal is © the Owner Societies 2010

View Online

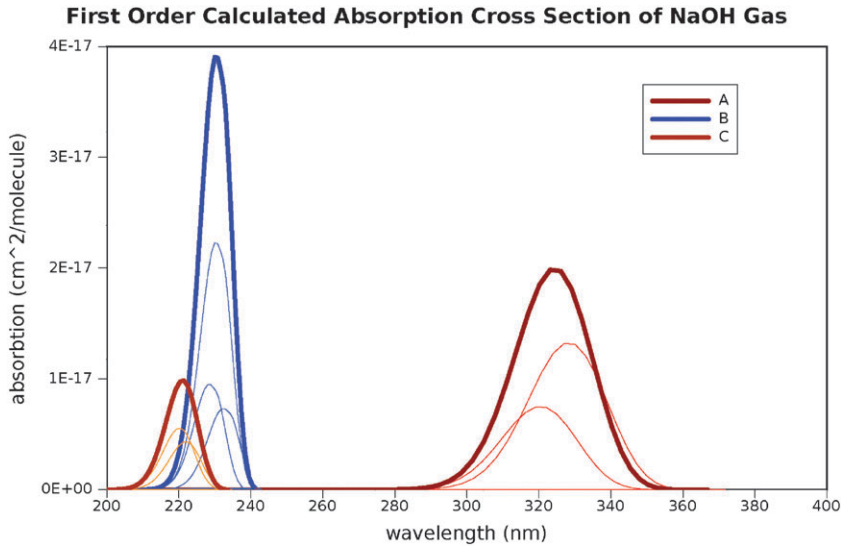

Fig. 6 The convoluted cross sections are shown in thick lines. This is the 1st order spectrum.

Table 5 Oscillator strengths calculated from the DVR cross sections. The single point values correspond to oscillator strengths from EOM-CCSD/POL calculation at the CCSD/POL equilibrium geometry. The ZPE values correspond to the cross section shown in Fig. 3 and ZPE + P1 correspond to the cross section shown in Fig. 6. The convoluted values correspond to the cross section shown in Fig. 7

Oscillator strength consistency check						
State	Single Point	ZPE	ZPE + P1	Convoluted	*f* exp. (200 K)	*f* exp. (300 K)
A	0.054	0.051	0.051	0.051	0.017	0.023
B	0.092	0.095	0.084	0.108	0.060	0.106
C	0.026	0.027	0.024			

geometry overlap (which corresponds to the maximum of the vibrational wavefunction) is given a weight factor of 0.50 and a weight factor of 0.25 is assigned to the two half-maximum points. Due to the symmetry in the bend, this distribution simplifies to 50% of the intensity coming from the point at the maximum and another 50% of the intensity coming from one of the points at the half-maximum.

Due to the breaking of the electronic degeneracy for states A and B, the distribution is 50% of the intensity coming from the point at the maximum, 25% of the intensity coming from one of the points at the half-maximum from one symmetry (A and B) and another 25% of the intensity coming from one of the points from the other symmetry (A′ and B′). Finally, the peaks are convoluted into one cross section for each excited state as shown in Fig. 6. The resulting convoluted spectrum is correct in the 1st order. Taking more points: 66%/33% Max would be 2nd order, 75%/50%/25% would be 3rd and so forth.

VI Temperature effects can be introduced at this stage

The spectrum in Fig. 6 does not have any temperature effects since only the first vibrational levels are populated. Temperature effects may be added by putting quanta into higher vibrational levels and recalculating the weights. No extra time is required for this as all Franck–Condon integrals are calculated at once. At 200 K the contribution from the second ground state vibrational level of the primary and the secondary modes to the absorption cross section is only about 10% of the total intensity which is not very noticeable. Only when the temperature used in determining the Boltzmann distribution is raised above 500 K does any significant change in peak intensity occur.

According to Self and Plane the significant increase in intensity for the peak at 220 nm is due to the increase in the Franck–Condon overlap. This assertion is based on the fact that their Configuration-Interaction Singles calculation (CIS/6-311+G(2d,p)) of the geometries of ground state and excited state showed that while the ground state in linear, the excited state is bent. In the present work, the ground state and excited state potential energy surfaces in Fig. 4 show a lack of a true double minimum on the excited state PES† which means that a linear geometry is preferred for the excited states in the energy range of the absorption cross section. Furthermore, the dipole strength for excitations B and C tends to diminish as a function of angle thereby reducing the total intensity (as opposed to increasing it). This is in support of the conclusion that hot bands originating from populating the bending mode will not lead to a significant increase in intensity for B and C states, but, possibly for A state. The higher intensity cross section observed by Self and Plane at 300 K may not be entirely due to a temperature dependence but to

† The energy surfaces in Figure Fig. 4 were calculated with the constraint that R_{NaO} is at it equilibrium. These surface were recomputed such that R_{NaO} and R_{OH} were allowed to relax and no double minimum was found. The geometry of State B was optimized using a Two-Determinant coupled cluster method[44,45] with POL basis set and was found to be linear.

Published on 15 June 2010 on http://pubs.rsc.org | doi:10.1039/C001906B
Downloaded on 17 August 2010

View Online

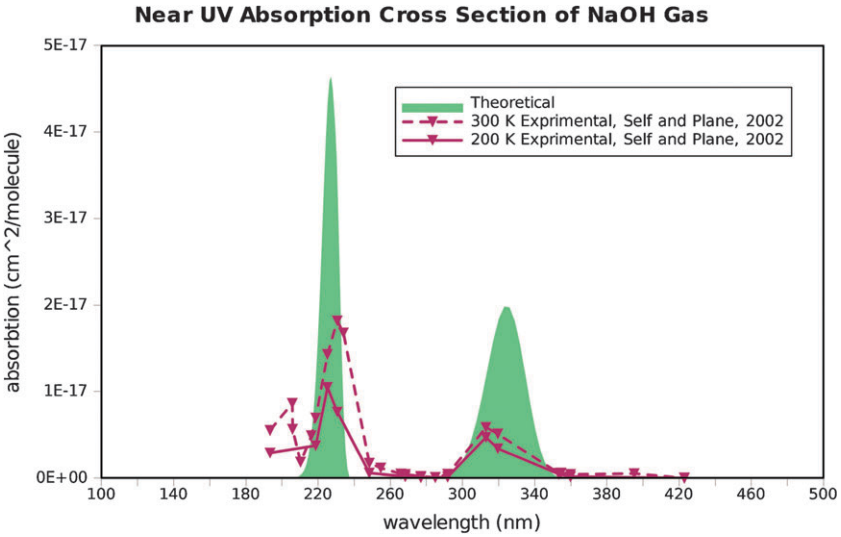

Fig. 7 The convoluted cross sections are shown in thick lines. This is the 1st order spectrum.

the fact that it is a higher resolution experiment and slightly more accurate.

The consistency check described in the Methods section is done and results presented in Table 5. It appears that as the peaks get broadened, the integrated oscillator strengths become slightly lower but no major discrepancies are noted. The final theoretical spectrum is presented in Fig. 7.

4 Discussion

There is good agreement for energies between the experimental absorption cross section and the calculated cross section for both peaks of experimental NaOH spectrum. The low energy excitation is more prone to error since any variation in the excitation energy due to choice of basis set was greatly amplified by the fact that the spectral range is in the near UV. This will be a recurring theme in atmospherically relevant molecules and special attention needs to be paid to get these low-energy excitations correctly.

The disagreement in intensity between theoretical and experimental spectra is more pronounced than the disagreement in energies. It stems from the fact that the calculated single point vertical excitation oscillator strengths do not match (refer to Table 5). Historically the agreement of oscillator strengths has always been good. The explanation of Self and Plane for the temperature dependence due to hot bands is not well supported by this study, so we are more likely to conclude that the increase in intensity observed from 200 K to 300 K is in fact due to the 300 K experiment being somehow more accurate. Table 5 includes the oscillator strengths from the 300 K experiment and shows that they are much closer to the theoretical oscillator strengths than the ones from the 200 K experiment.

It is important to note that all of the calculated energy surfaces which are accessible in the UV/vis spectral range are radical-type dissociations. The excited states which lead to ionic dissociation have excitation energies closer to the vacuum UV spectral range (100s nm) and are not treated in this work. Ionic dissociation cross section can be done in the same fashion as described here provided one uses electronic structure methods appropriate for charge transfer PESs.

There are a few points to stress in making this procedure work for large molecules. It is not presently cost effective to use the larger basis sets for these molecules but will become increasingly possible with further development of the parallel ACES III[46] program. This will also make it possible to do calculations at the CCSDT (and higher) level of theory. From Fig. 3 it is obvious that by using the POL basis set one can incur up to ~20 nm error in energy (compared to a larger WMR basis set) but the intensities remain almost constant. There will also be times where even a POL basis set will be too large to be practical. For cases such as these, it is recommended that the chromophore be treated separately from the rest of the molecule and the energy shifts from a low cost basis set to the larger basis set be determined. This suggestion will work for localized excitations but would not be accurate for excitations involving charge transfer or large conjugated systems.

Aside from the errors in the electronic structure calculations there are also errors incurred by selectively discarding vibrational degrees of freedoms using the criteria described in the methodology section. It is presently unclear what that error is since no other procedure which treats dissociative potentials and multiple degrees of freedom is currently available. Since the approach used here works for dissociative as well as bound potentials a study will be forthcoming where our method will be compared with either VIBRON or HOTFCHT for obtaining an absorption cross section of a bound excited state to determine the errors and to investigate any possible fixes.

Acknowledgements

The authors would like to thank the United States Air Force Office of Scientific Research (AFOSR-F49620 01-1-0072) for their financial support. Special thanks goes to G. T. Drozd and N. M. Donahue for pointing out the need for reliable *ab initio* predictions of absorption cross sections in the atmospheric science community.

Published on 15 June 2010 on http://pubs.rsc.org | doi:10.1039/C001906B
Downloaded on 17 August 2010

 This journal is © the Owner Societies 2010

View Online

References

1 S. Madronich, D. R. Hastie, B. A. Ridley and H. I. Schiff, *J. Atmos. Chem.*, 1984, **1**, 151–157.
2 E. Mayor and A. M. Velasco, *J. Geophys. Res.*, 2007, **112**, D13304.
3 M. E. Jenkin, A. A. Boyd and R. Lesclaux, *J. Atmos. Chem.*, 1998, **29**, 267–298.
4 J. M. Flaud, C. C. Peyret, J. W. C. Johns and B. Carli, *J. Chem. Phys.*, 1989, **91**, 1504–1510.
5 J. Koput, *Chem. Phys. Lett.*, 1995, **236**, 516–520.
6 M. Nooijen and A. Hazra, *VIBRON-A Program for Vibronic Coupling and Franck–Condon Calculations. With contributions from J. F. Stanton and K. Sattelmeyer.*, 2003.
7 R. Berger, C. Fischer and M. Klessinger, *J. Phys. Chem. A*, 1998, **102**, 7157–7167.
8 R. J. Le Roy, *LEVEL 8.0, A Computer Program for Solving the Radial Schrödinger Equation for Bound and Quasibound Levels.*
9 J. M. C. Plane, *Ann. Geophys.*, 2000, **18**, 807–814.
10 L. Andrews, *J. Mol. Spectrosc.*, 1976, **61**, 337–345.
11 D. E. Self and J. M. C. Plane, *Phys. Chem. Chem. Phys.*, 2002, **4**, 16–23.
12 J. Čižek, *Adv. Chem. Phys.*, 1969, **14**, 35.
13 J. Čižek, J. Paldus and I. Shavitt, *Phys. Rev. A: At., Mol., Opt. Phys.*, 1972, **1**, 50.
14 R. J. Bartlett and G. D. Purvis III, *Int. J. Quantum Chem.*, 1978, **14**, 561.
15 R. J. Bartlett and G. D. Purvis III, *Phys. Scr.*, 1980, **21**, 255.
16 G. D. Purvis III and R. J. Bartlett, *J. Chem. Phys.*, 1982, **76**, 1910–1918.
17 Y. S. Lee, S. A. Kucharski and R. J. Bartlett, *J. Chem. Phys.*, 1984, **81**, 5906–5912.
18 R. J. Bartlett, *J. Phys. Chem.*, 1989, **93**, 1697–1708.
19 R. J. Bartlett and J. F. Stanton, in *Applications of post-Hatree-Fock methods: a tutorial*, ed. D. Boyd and K. Lipkowitz, VCH Publishers, New York, 1994, pp. 65–169.
20 R. J. Bartlett, in *Coupled cluster theory: An overview of recent developments*, ed. D. R. Yarkony, World Scientific Publishing Co. Ltd., Singapore, 1995, pp. 1047–1131.
21 J. Paldus, in *Methods in Computational Molecular Physics*, ed. S. Wilson and G. H. F. Diercksen, Plenum Press, New York, 1992, p. 99.
22 J. F. Stanton and R. J. Bartlett, *J. Chem. Phys.*, 1993, **98**, 7029.
23 M. Nooijen and R. J. Bartlett, *J. Chem. Phys.*, 1997, **106**, 6441–6448.
24 J. F. Stanton, J. T. J. Gauss, S. A. Perera, J. D. Watts, A. D. Yau, M. Nooijen, N. Oliphant, P. G. Szalay, W. J. Lauderdale, S. R. Gwaltney, S. Beck, A. Balkova, D. E. Bernholdt, K. K. Baeck, P. Rozyczko, H. Sekino, C. Huber, J. Pittner and W. Cencek, *ACES II is A Program Product Of The Quantum Theory Project University Of Florida. packages Included Are VMOL (J. Almlof, P. R. Taylor); VPROPS (P. Taylor); ABACUS (T. Helgaker, H. J. Aa. Jensen, P. Jørgensen, J. Olsen, P. R. Taylor); HONDO/GAMESS (M. W. Schmidt).*
25 J. C. Light, I. P. Hamilton and J. V. Lill, *J. Chem. Phys.*, 1985, **82**, 1400–1409.
26 P. Puzari, R. S. Swathi, B. Sarkar and S. Adhikari, *J. Chem. Phys.*, 2005, **123**, 134317.
27 H.-G. Yu, *J. Chem. Phys.*, 2005, **122**, 164107.
28 G. Rauhut, *J. Chem. Phys.*, 2004, **121**, 9313–22.
29 D. T. Colbert and W. H. Miller, *J. Chem. Phys.*, 1992, **96**, 1982–1991.
30 M. Monnerville and J. M. Robbe, *J. Chem. Phys.*, 1994, **101**, 7580–7591.
31 C. C. Marston, G. Balint-Kurti and Gabriel, *J. Chem. Phys.*, 1989, **91**, 3571–3576.
32 G. Balint-Kurti, Gabriel, S. P. Mort and C. C. Marston, *Comput. Phys. Commun.*, 1993, **74**, 289–296.
33 J. G. Calvert and J. N. Pitts Jr., *Photochemistry*, John Wiley & Sons, New York, 1966.
34 A. Bolovinos, P. Tsekeris, J. Philis, E. Pantos and G. Andritsopoulos, *J. Mol. Spectrosc.*, 1984, **103**, 240–256.
35 B. A. Flowers, J. F. Stanton and W. R. Simpson, *J. Phys. Chem. A*, 2007, **111**, 11602–11607.
36 F. D. Pope, J. C. Hansen, K. D. Bayes, R. R. Friedl and S. P. Sander, *J. Phys. Chem. A*, 2007, **111**, 4322–4332.
37 A. J. Sadlej, *Theor. Chim. Acta*, 1991, **79**, 123–140.
38 P. Kuijpers, T. Törring and A. Dymanus, *Chem. Phys.*, 1976, **15**, 457–461.
39 E. P. F. Lee and T. G. Wright, *J. Phys. Chem. A*, 2002, **106**, 8903–8907.
40 T. H. Dunning Jr., *J. Chem. Phys.*, 1989, **90**, 1007–1023.
41 D. E. Woon and T. H. Dunning Jr., *J. Chem. Phys.*, 1995, **103**, 4572–4585.
42 P. O. Widmark, P. A. Malmqvist and B. O. Roos, *Theor. Chim. Acta*, 1990, **77**, 291–306.
43 N. Acquista and S. Abramowitz, *J. Chem. Phys.*, 1969, **51**, 2911–2914.
44 P. G. Szalay and R. J. Bartlett, *J. Chem. Phys.*, 1994, **101**, 4936–4944.
45 A. Balková and R. J. Bartlett, *Chem. Phys. Lett.*, 1992, **193**, 364–372.
46 V. F. Lotrich, N. Flocke, M. Ponton, A. D. Yau, A. Perera, E. Deumens and R. J. Bartlett, *J. Chem. Phys.*, 2008, **128**, 194104.

Published on 15 June 2010 on http://pubs.rsc.org | doi:10.1039/C001906B
Downloaded on 17 August 2010